Global Sensitivity of Tropospheric Ozone to Precursor Emissions in Clean and Present-Day Atmospheres: Insights from AerChemMIP Simulations

Wei Wang[1] and Chloe Yuchao Gao[2,3,*]

[1] Nanjing-Helsinki Institute in Atmospheric and Earth System Sciences, Nanjing University, Nanjing, 210023, China

[2] Department of Atmospheric and Oceanic Sciences & Shanghai Key Laboratory of Ocean-Land-Atmosphere Boundary Dynamics and Climate Change, Fudan University, Shanghai, 200438, China

[3] Institute of Eco-Chongming (IEC), Shanghai, 202151, China

[*] Corresponding author: Chloe Yuchao Gao (gyc@fudan.edu.cn)

Abstract

Ozone (O_3) is a Short-lived Climate Forcer (SLCF) that contributes to radiative forcing and indirectly affects the atmospheric lifetime of methane, a major greenhouse gas. This study investigates the sensitivity of global O_3 to precursor gases in a clean atmosphere, where hydroxyl (OH) radical characteristics are more spatially uniform than in present-day conditions, using data from the *PiClim* experiments of the Aerosols and Chemistry Model Intercomparison Project (AerChemMIP) within the CMIP6 framework. We also evaluate the O_3 simulation capabilities of four Earth system models (CESM2-WACCM, GFDL-ESM4, GISS-E2-1-G, and UKESM1-0-LL). Our analysis reveals that the CESM and GFDL models effectively capture seasonal O_3 cycles and consistently simulate vertical O_3 distribution. While all models successfully simulate O_3 responses to anthropogenic precursor emissions, CESM and GFDL show limited sensitivity to enhanced natural NO_x emissions (e.g., from lightning) compared to GISS and UKESM. The sensitivities of O_3 to its natural precursors (NO_x and VOCs) in GISS and UKESM models are substantially lower than their responses to anthropogenic emissions, particularly for lightning NO_x sources. These findings refine our understanding of O_3 sensitivity to natural precursors in clean atmospheres and provide insights for improving O_3 predictions in Earth system models.

1 Introduction

Tropospheric ozone (O_3) is a key air pollutant and atmospheric oxidant, exerting extensive influence on air quality and human health (Coffman et al., 2024; Lim et al., 2019; Malley et al., 2017; Nuvolone et al., 2018), climate systems, and biogeochemical processes (Hu et al., 2023; Fowler et al., 2009). As a Short-lived Climate Forcer (SLCF), tropospheric O_3 exerts a radiative forcing of 0.35–0.5 W m^{-2} and influences atmospheric processes such as evaporation, cloud formation, and general circulation (Khomsi et al., 2022; Möller and Mauersberger, 1992; Rogelj et al., 2014; Stevenson et al., 2013). Furthermore, O_3 plays a crucial role in regulating the terrestrial carbon sink and enhancing the formation of the hydroxyl (OH) radical (Naik et al., 2013b), which, in turn, affect the lifetime of methane (and halocarbons), the second most prominent anthropogenic greenhouse gas after carbon dioxide (Kumaş et al., 2023). O_3 also contributes to an increased atmospheric oxidation capacity, influencing the formation of secondary aerosols, such as organic aerosol, sulfate, and nitrate, which have significant implications for radiative forcing (Karset et al., 2018).

While stratospheric O_3 entrainment contributes to tropospheric O_3 levels, the primary source of tropospheric O_3 is photochemical production. This secondary pollutant is formed through photochemical oxidation reactions involving oxides of nitrogen ($NO + NO_2 = NO_x$) and volatile organic compounds (VOCs) in the presence of OH and hydroperoxyl (HO_2) radicals (Monks et al., 2015). The relationship between O_3 and its precursors is nonlinear, making it challenging to mitigate O_3 pollution through simple precursor reduction strategies. Regional-scale sensitivity to O_3 precursors has been extensively investigated, such as emphasizing the diagnostic utility of ratios including O_3/NO_x (Jin et al., 2023; Sillman and He, 2002) and VOC/NO_x (Li et al., 2024) for assessing O_3-NO_x-VOC sensitivity, and nations such as the United Kingdom and the United States have demonstrated significant success in controlling regional ozone levels by implementing measures to reduce NO_x emissions (Hakim et al., 2019). However, the global-scale sensitivity of O_3 to its precursors has received limited attention, despite evidence suggesting that global O_3 forcing may have a more substantial impact on climate forcing than localized O_3 enhancements. Consequently, improving our understanding of O_3 formation

mechanisms on a global scale is essential for effective air quality management and climate change mitigation strategies (Yu et al., 2021).

Recent studies utilizing Coupled Model Intercomparison Project Phase 6 (CMIP6; Eyring et al., 2016) datasets have offered insights into the spatio-temporal evolution of the global tropospheric O_3 budget from 1850 to 2100 (Griffiths et al., 2021; Turnock et al., 2019) and have quantified the global stratosphere-troposphere O_3 exchange process (Li et al., 2024; Griffiths et al., 2021). However, challenges persist in quantifying the sensitivity of global O_3 to its precursors when assessing the increasing global O_3 forcing attributed to these precursors. These challenges arise from regional variability in meteorological conditions (Carrillo-Torres et al., 2017), differences in NO_x and VOC volume mixing ratios (Jin et al., 2023; Sillman and He, 2002), and the distinct characteristics of OH and HO_2 influenced by varying degrees of urbanization (Karl et al., 2023; Vermeuel et al., 2019). Furthermore, while the observed upward trends in O_3 levels are primarily attributed to increased precursor emissions, limited research has investigated whether contemporary atmospheric conditions—shaped by climate warming and enhanced oxidation capacities—may be creating a more favorable environment for O_3 formation.

To address these gaps, this study investigates the sensitivity of global-scale O_3 to its precursors under a pre-industrial background atmosphere, with approximate uniform HO_x conditions in major continental areas. We also examine the feedback mechanisms of different model responses to precursors from both anthropogenic and natural sources, using *PiClim* experiment data from the Aerosols and Chemistry Model Intercomparison Project (AerChemMIP) simulations (Collins et al., 2017) within CMIP6. Additionally, this research evaluates the ozone formation potential in the pre-industrial era based on contemporary (2014) emissions of O_3 precursors, with the aim of elucidating whether shifts in the background atmosphere have rendered it chemically more conducive to O_3 generation. Our analysis employs four models with interactive stratospheric and tropospheric chemistry, which have been extensively utilized in O_3-related research (Brown et al., 2022; Griffiths et al., 2021; Tilmes et al., 2022; Zeng et al., 2022). This approach allows us to assess the global-scale sensitivity of O_3 to its precursors, evaluate the consistency and discrepancies among different models in representing O_3-precursor relationships, and provide insights into

the potential impacts of changing emissions on future global O_3 levels and associated climate forcing, contributing to more accurate projections of future climate change.

2 Models and methods

2.1 Model descriptions

We use monthly-mean simulation data from four Earth system models in this study. The four chosen models possess the benefit of extensive applicability and a comprehensive *PiClim* computational framework. Table 1 summarizes key model features, including model resolution, vertical stratification, complexity of gas-phase chemistry, and relevant references. All models include interactive coupling of tropospheric and stratospheric chemistry with O_3 dynamics integrated into the radiation scheme, simulating the interaction between O_3 concentration and temperature. The response of simulated reactive gas emissions to chemical complexity is important. For example, changes in Biogenic Volatile Organic Compounds (BVOCs) can impact O_3, methane lifetime, and potentially the oxidation of other aerosol precursors in models with interactive tropospheric chemistry via OH changes.

Table 1. Information on model resolution, vertical levels, property of gas-phase chemistry and references.

Model	Resolution (lat × lon)	Number of gridpoints	Vertical levels	Aerosol model	Simulation reference
CESM2-WACCM	192 × 288	55296	70 levels; top level 6×10^{-6} hPa	MAM4	(Gettelman et al., 2019)
GFDL-ESM4	180 × 288	51840	49 levels; top level 0.01 hPa	MATRIX	(Dunne et al., 2020; Horowitz et al., 2020)
GISS-E2-1-G	90 × 144	12960	40 levels; top level 0.1 hPa	OMA	(Miller et al., 2014; Kelley et al., 2020)
UKESM1-0-LL	144 × 192	27648	85 levels; top level 1 hPa	GLOMAP	(Mulcahy et al., 2018; Sellar et al., 2019)

CESM2-WACCM (hereafter "CESM") is a fully coupled Earth system model that integrates the Community Earth System Model version 2 (Emmons et al., 2020) with the Whole Atmosphere Community Climate Model version 6 (WACCM6). The atmospheric component operates at a horizontal resolution of 0.9375° latitude by 1.25° longitude, with 70 hybrid sigma-pressure vertical layers extending from the surface to 6×10^{-6} hPa. Its interactive chemistry and aerosol modules include the troposphere, stratosphere, and lower thermosphere, with a comprehensive treatment of 231 species, 150 photolysis reactions, 403 gas-phase reactions, 13 tropospheric heterogeneous reactions, and 17 stratospheric heterogeneous reactions (Emmons et al., 2020). The model utilizes the four-mode Modal Aerosol Model (MAM4) (Emmons et al., 2020) and features its secondary organic aerosol (SOA) framework based on the Volatility Basis Set (VBS, Donahue et al., 2013) approach. The photolytic calculations use both inline chemical modules and a lookup table approach, which does not consider changes in aerosols.

The Atmospheric Model version 4.1 (AM4.1, Horowitz et al. (2020)) within the GFDL Earth system model (Dunne et al., 2020) incorporates an interactive chemistry scheme that spans both the troposphere and stratosphere (GFDL-ESM4; hereafter "GFDL"). The atmospheric component operates at a horizontal resolution of 1° latitude by 1.25° longitude, with 49 hybrid sigma-pressure vertical layers extending from the surface to 0.01 hPa. This scheme includes 56 prognostic tracers, 36 diagnostic species, 43 photolysis reactions, 190 gas-phase kinetic reactions, and 15 heterogeneous reactions. Stratospheric chemistry accounts for key O_3 depletion cycles (O_x, HO_x, NO_x, ClO_x, and BrO_x) and heterogeneous reactions on stratospheric aerosols (Austin et al., 2013). Photolysis rates are calculated dynamically with the FAST-JX version 7.1 code, which considers the radiative impacts of modeled aerosols and clouds. The chemical mechanism is further elaborated in Horowitz et al. (2020), and the gas-phase and heterogeneous chemistry are similar to those employed by Schnell et al. (2018). Non-interactive natural emissions of O_3 precursors are prescribed as outlined in Naik et al. (2013a).

The GISS model, developed by the NASA Goddard Institute for Space Studies, integrates the chemistry-climate model version E2.1 with the GISS Ocean v1 (G01) model (GISS-E2-1-G; hereafter "GISS"). The specific configurations of this model

utilized for the CMIP6 are detailed in Kelley et al. (2020). In this study, we focus on the model subset that includes online interactive chemistry. The atmospheric component operates at a horizontal resolution of 2° latitude by 2.5° longitude, with 40 hybrid sigma-pressure vertical layers extending from the surface to 0.1 hPa. The interactive chemistry module employs the GISS Physical Understanding of Composition-Climate Interactions and Impacts (G-PUCCINI) mechanism for gas-phase chemistry (Kelley et al., 2020; Shindell et al., 2013). For aerosols, the model utilizes either the One-Moment Aerosol (OMA) or the Multiconfiguration Aerosol Tracker of Mixing state (MATRIX) model (Bauer et al., 2020). The gas-phase chemistry involves 146 reactions, including 28 photodissociation reactions, affecting 47 species across the troposphere and stratosphere, along with an additional five heterogeneous reactions. The model transports 26 aerosol particle tracers and 34 gas-phase tracers (OMA).

UKESM represents the United Kingdom's Earth system model (Sellar et al., 2019). It builds upon the Global Coupled 3.1 (GC3.1) configuration of HadGEM3 (Williams et al., 2018), incorporating additional Earth system components, such as ocean biogeochemistry, the terrestrial carbon-nitrogen cycle, and atmospheric chemistry (UKESM1-0-LL; hereafter "UKESM"). Walters et al. (2019) provided descriptions of the atmospheric and land components. The atmospheric component operates at a horizontal resolution of 1.25° latitude by 1.875° longitude, with 85 vertical layers extending from the surface to 85 km. The chemistry module in the UKESM model is a unified stratosphere-troposphere scheme (Archibald et al., 2020) including 84 tracers, 199 bimolecular reactions, 25 unimolecular and termolecular reactions, 59 photolytic reactions, 5 heterogeneous reactions, and 3 aqueous-phase reactions for the sulfur cycle from the United Kingdom Chemistry and Aerosols (UKCA) model. The aerosol module is based on the two-moment scheme from UKCA, known as GLOMAP mode, and is integrated into the Global Atmosphere 7.0/7.1 configuration of HadGEM3 (Walters et al., 2019). The UKESM uses interactive Fast-JX photolysis scheme, which is applied to derive photolysis rates between 177 and 850 nm, as described in Telford et al. (2013). In the lower mesosphere, photolysis rates are calculated using lookup tables (Lary and Pyle, 1991).

Models differ in their representation of O_3 source and sink processes, as well as in the definitions of the associated budget terms, which contributes to variability in

model outcomes (Stevenson et al., 2006; Young et al., 2018). For example, in the GISS model, the tropospheric chemistry component simulates the NO_x-HO_x-O_x-CO-CH_4 system and the oxidation pathways for non-methane volatile organic compounds (NMVOCs). Central to these discrepancies are the treatments of non-methane volatile organic compound NMVOCs chemistry, which impacts both chemical production and destruction rates, along with surface removal mechanisms and stratospheric influences. Furthermore, the choice of tropopause definition can significantly alter the diagnosed O_3 burden, as well as the flux from the stratosphere.

All four of the interactive tropospheric chemistry models contain parameterizations of the nitrogen oxide (NO_x) emissions from lightning based on the height of the convective cloud top (Price et al., 1997; Price and Rind, 1992; Price, 2013), and the tropopause height for each model based on the WMO definition. Each model has a different way of implementing emissions and how much they are profiled. For instance, online calculations of lightning NO_x emissions during deep convection in the GISS model are based on the method described by (Kelley et al., 2020). Lightning NO_x continues to be a major source of uncertainty in both model comparisons and the temporal development of tropospheric O_3 because it has a disproportionately significant influence on tropospheric-O_3 concentration relative to surface emissions (Murray et al., 2013).

BVOC emissions are modeled as a function of vegetation type and cover, as well as temperature and photosynthetic rates (gross primary productivity) (Unger, 2014; Sporre et al., 2019; Pacifico et al., 2011; Guenther et al., 1995). While models vary in the speciation of emitted VOCs, they commonly include isoprene and monoterpenes, each with its own distinct emission parameterization. Despite the common reliance on photosynthetically active radiation for the parameterization of BVOC emissions across the four models, there exist notable distinctions. For instance, the GFDL model exclusively considers the leaf area index, neglecting the impact of temperature on BVOC emissions, and the CESM, GISS, and UKESM models omit the influence of vegetation type from their calculations.

2.2 Simulation data and experimental design

The primary objective of AerChemMIP is to quantitatively ascertain the influence of aerosols and reactive trace gases on the climate system, as well as the

bidirectional feedback mechanisms involved (Collins et al., 2017). Table 2 presents a synopsis of the experimental configurations employed in this study. The control experiment, denoted as *PiClim-control*, is designed to stabilize both atmospheric composition and climatic conditions at a state reminiscent of the pre-industrial era, where the natural fractions of stratospheric ozone forcing species such as halocarbons was extremely low, specifically 1850. The *PiClim-2x* experiment involves doubling of individual natural emission fluxes relative to the 1850 control, while the *PiClim-x* experiments calibrate these fluxes to align with the emission levels prevalent in 2014 (Collins et al., 2017). *PiClim-2x*NO_x represents to doubling of the nitric oxide emissions from natural sources due to lightning activity. *PiClim-2xVOC* represents to doubling of the volatile organic compound emissions from natural sources, including isoprene and monoterpenes. *PiClim-HC* represents the pre-industrial climatological control with 2014 halocarbons emissions both from anthropogenic (CFCs, HCFCs and compounds containing bromine) and natural sources. *PiClim-*CH_4 represents the pre-industrial climatological control with 2014 methane emissions both from anthropogenic and natural sources. *PiClim-*NO_x represents the pre-industrial climatological control with 2014 nitrogen oxide emissions both from anthropogenic and natural sources. *PiClim-VOC* represents the pre-industrial climatological control with 2014 VOC emissions both from anthropogenic and natural sources. *PiClim-NTCF* represents the pre-industrial climatological control with 2014 near-term climate forcers emissions, including aerosols and chemically reactive gases such as tropospheric ozone and methane. *PiClim-*N_2O represents the pre-industrial climatological control with 2014 nitrous oxide emissions both from anthropogenic and natural sources. *PiClim-aer* represents the pre-industrial climatological control with 2014 aerosol concentrations. *PiClim-* O_3 represents the pre-industrial climatological control with 2014 ozone concentrations. *PiClim-BC* represents the pre-industrial climatological control with 2014 black carbon concentrations.

238 **Table 2.** The available experiments of selected models in this study. "X" represents the experiment is available

Model \ *PiClim-*	*2xNO$_x$*	*2xVOC*	*HC*	*CH$_4$*	*NO$_x$*	*VOC*	*NTCF*	*N$_2$O*	*O$_3$*	*aer*	*control*	*BC*
CESM2-WACCM	X	X	X	X	X	X	X	X				
GFDL-ESM4	X	X	X		X	X			X	X	X	X
GISS-E2-1-G	X	X	X	X	X	X	X	X	X	X	X	X
UKESM1-0-LL	X	X	X	X	X	X	X	X	X	X	X	X

239

We analyzed models that had archived sufficient data in the Earth System Grid Federation (ESGF) system to permit accurate characterization of tropospheric O_3. In practice this meant we used archived O_3 data from the AERmon characterization of the tropospheric O_3 (variable name: "o3") on native model grids. Other variables used include chemical production (variable name: "o3prod"), chemical destruction (variable name: "o3loss"), nitrogen monoxide (variable name: "no"), nitrogen dioxide (variable name: "no2"), isoprene (variable name: "isop"), organic dry aerosol (variable name: "emioa"), and secondary organic aerosol (variable name: "mmrsoa"). All data used in this paper are available on the Earth System Grid Federation website and can be downloaded from https://esgf-index1.ceda.ac.uk/search/cmip6-ceda/ (last access: 4 July 2024, ESGF-CEDA, 2020).

A new set of historical anthropogenic emissions has been developed with the Community Emissions Data System (CEDS, Hoesly et al., 2018). CEDS uses updated emission factors to provide monthly emissions of the major aerosol and trace gas species over the period 1750 to 2014 for use in CMIP6, and biomass burning emissions are based on a different inventory developed separate from CEDS (Van Marle et al., 2017). The primary analysis examines emissions of NO_x and VOCs from anthropogenic (Hoesly et al., 2018) and biomass burning sources (van Marle et al., 2017) that were provided as a common emission inventory to be used by all models (including the four in this study) in CMIP6 simulations. In the CESM and GFDL models, biogenic emissions, including isoprene and monoterpenes, are calculated interactively using MEGAN version 2.1 (Guenther et al., 2012) and are further utilized for SOA formation. While in the GISS model, biogenic emissions of isoprene are computed online and are sensitive to temperature (Shindell et al., 2006), whereas alkenes, paraffins, and terpenes are prescribed. And in the UKESM model, emissions of isoprene and monoterpenes are interactively calculated using the iBVOC emission model (Pacifico et al., 2011).

3 Results and Discussions

3.1 Spatial, seasonal, and vertical distribution of tropospheric O_3

We first investigate the seasonal and vertical variations of ozone volume mixing ratio in the pre-industrial atmospheres simulated by four selected models. The analysis of tropospheric O_3 data derived from the *PiClim* experiment outcomes of

CMIP6 models reveals distinct seasonal cycles and inter-model variations (Fig. 1). The GISS model demonstrates the highest simulated tropospheric column O_3 volume mixing ratio at 50.29 ppbv in the 29th and 30th year of simulation, followed by the UKESM (44.50 ppbv), CESM (38.02 ppbv), and GFDL (31.03 ppbv), where the height of the tropopause is based on the definition of WMO. These are consistent with previous findings from historical experiments (Griffiths et al., 2021).

Furthermore, our analysis indicates that the disparity in O_3 volume mixing ratio during the *PiClim* experiment primarily occurs in polar regions. This may be attributed to the GISS model's ability to replicate a more robust entrainment of stratospheric O_3, a key source of tropospheric O_3 in the pre-industrial atmosphere, particularly at the poles. Previous studies have demonstrated that elevated O_3 levels in the Arctic during MAM and DJF, as well as in the Antarctic during JJA and SON, result from the cumulative impact of the polar O_3 barrier (Romanowsky et al., 2019).

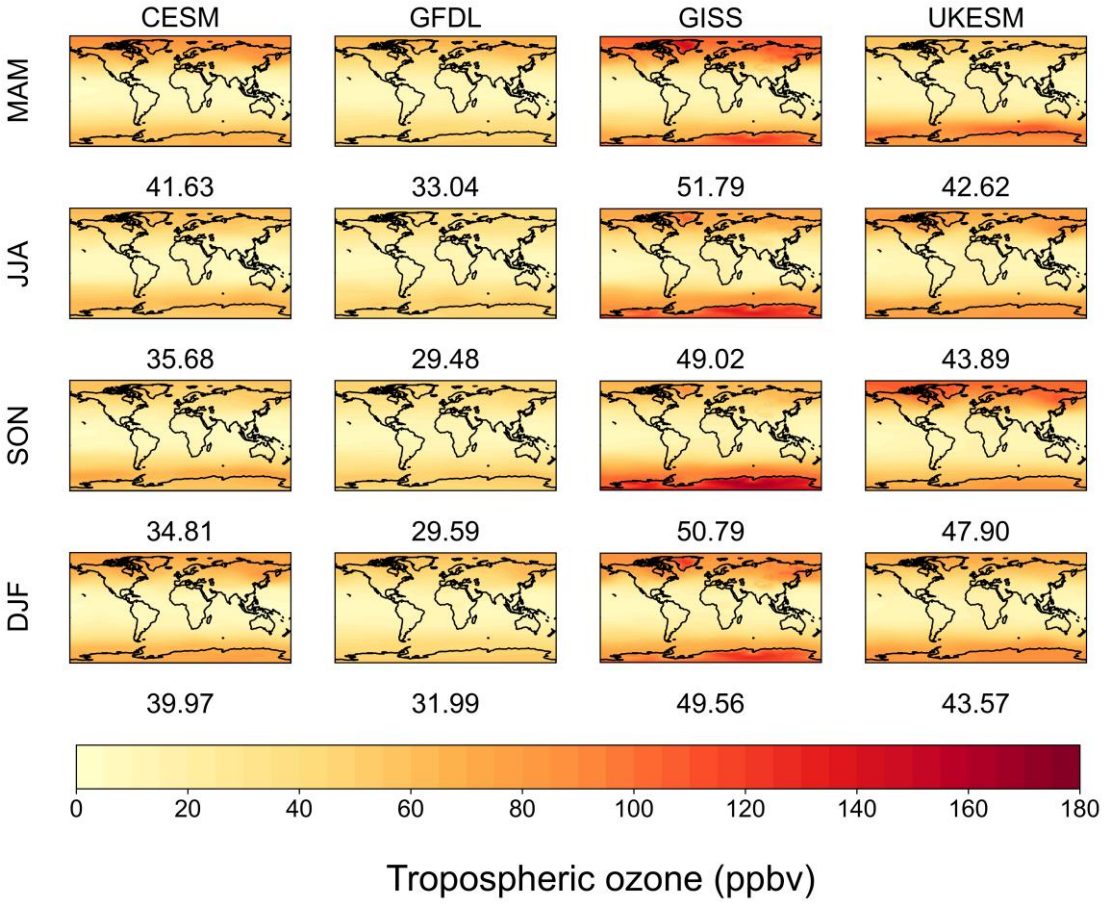

Figure 1. Comparison of the seasonal cycle of tropospheric column averaged volume mixing ratio of O_3 (density weighted) of the *PiClim* experiment results in the 29th and 30th year of simulation of the four models. Each row shows a separate meteorological season, arranged from top to bottom: March to May (MAM), June to August (JJA),

September to November (SON), and December to February (DJF). Each column represents a selected model, listed from left to right: CESM, GFDL, GISS, and UKESM. The figures displayed below each chart represent the global average ozone volume mixing ratio.

Seasonal variations in tropospheric O_3 volume mixing ratio exhibit model-specific patterns. The CESM, GFDL, and GISS models simulate peak tropospheric O_3 volume mixing ratio in spring during the *PiClim* experiments. In contrast, the UKESM model reproduces maximum O_3 volume mixing ratio in autumn, indicating a limited capability in simulating dynamic circulations in the tropopause. Furthermore, the seasonal O_3 cycle simulations in CESM, GFDL, and GISS exhibit distinct discrepancies in their outcomes. For instance, the CESM model simulates the lowest O_3 volume mixing ratio in SON, while the GFDL model exhibits the lowest volume mixing ratio in JJA. The GISS model simulation indicates higher O_3 levels in autumn compared to DJF, which is consistent with results from historical experiments (Griffiths et al., 2021). Additionally, our analysis reveals that the CESM simulations demonstrate the most pronounced seasonal oscillation amplitude in O_3 volume mixing ratio, approximately 6.82 ppbv. This feature underscores the model's sensitivity to seasonal factors affecting tropospheric O_3 dynamics.

In the *PiClim* experiments, all four models accurately reproduce the peak volume mixing ratio of O_3 in the middle stratosphere at 10 hPa and the zonal average mixing ratios reaching their peak in the upper troposphere, particularly in extratropical regions, indicative of extended chemical lifetimes at higher altitudes. However, notable disparities are observed in the vertical distribution characteristics of O_3 among the four models (Fig. 2). Specifically, the CESM model exhibits the highest vertical extension, including an additional hotspot simulated in the thermosphere. While the GFDL and CESM2 models exhibit consistent simulation outcomes below 0.01 hPa, GISS and UKESM simulate significantly higher stratospheric O_3 levels at 10 hPa in comparison.

Notable distinctions are observed in the spatial distribution of O_3. The GISS model simulates a more vertically concentrated and latitudinally extended O_3 distribution. This characteristic may be a crucial factor contributing to the pronounced impact of O_3 transport in the polar stratosphere, as simulated by GISS. The zonal variability in O_3 distribution simulated by the UKESM falls between that of the GISS and CESM models. These inter-model discrepancies in O_3 simulation results likely

reflect suboptimal representation of local and regional dynamics, as well as omitted chemical processes in corresponding models. The variability and uncertainty in O_3 precursor emission estimates further exacerbate these disparities.

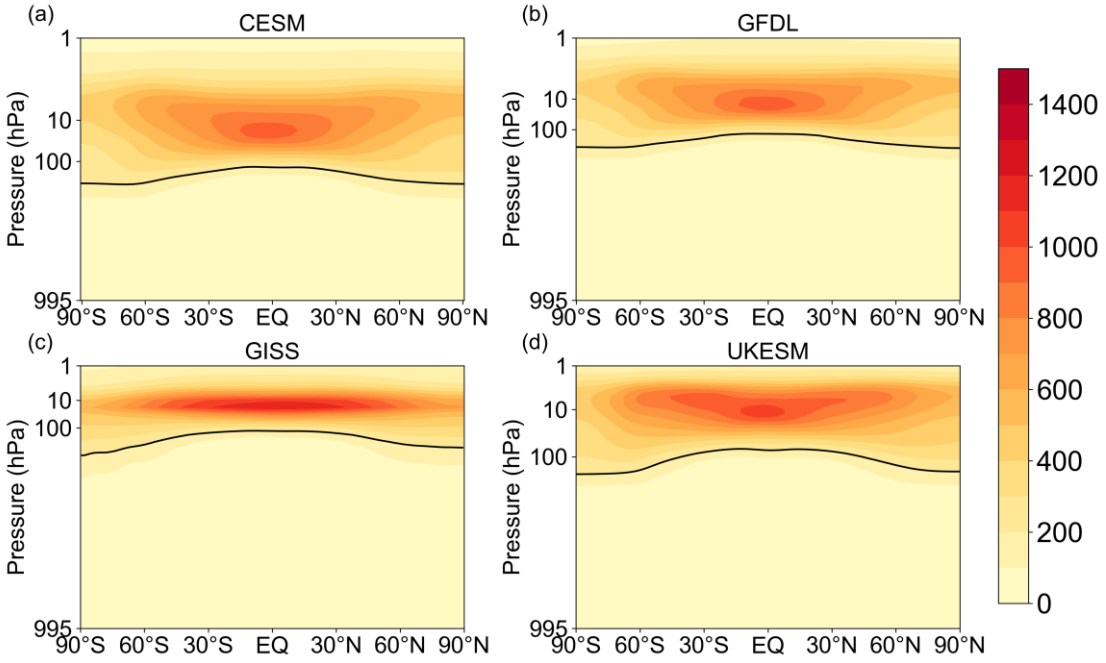

Figure 2. The zonal mean O_3 distribution for the 29th and 30th year of the *PiClim* experiment results from the (a) CESM, (b) GFDL, (c) GISS, and (d) UKESM model. Thick black lines represent the tropopause height for each model based on the WMO definition.

3.2 Characteristics of tropospheric O_3 under various experiments

Tables 3 and 4 present the global O_3 volume mixing ratio and tropospheric O_3 volume mixing ratio across all experiments from the four different models. The GISS model simulations show higher tropospheric O_3 volume mixing ratios, reflecting increased rates of stratospheric downwelling and surface O_3 precursor emissions. However, its overall O_3 volume mixing ratio is notably lower compared to the UKESM, CESM, and GFDL models, with reductions of 114.24, 76.16, and 47.04 ppbv, respectively. Analysis reveals that in the CESM, GFDL, and GISS models, the global O_3 molar fraction in the *PiClim-2NO$_x$* and *PiClim-NO$_x$* experiments surpasses that in the *PiClim-2VOC* and *PiClim-VOC* experiments. This difference is most pronounced in the GISS model, aligning with previous findings indicating its heightened sensitivity to NO_x response (Turnock et al., 2019). Conversely, in the UKESM model, the global O_3 molar fraction of the *PiClim-2NO$_x$* experiment is lower than that of the *PiClim-2VOC* experiment. Interestingly, the tropospheric O_3 volume mixing ratios in the *PiClim-2NO$_x$* experiment in the CESM and GFDL models

are notably lower than in their respective *PiClim-2VOC* experiments, with reductions of 0.41 and 0.29 ppbv. This discrepancy challenges the conventional understanding that increased NO_x emissions from lightning activity should lead to tropospheric O_3 generation, suggesting a need for enhanced sensitivity simulations in these two models regarding O_3 and NO_x emissions from natural sources due to lightning activity. In contrast, the *PiClim-2NO$_x$* experiments of the GISS and UKESM models effectively simulate an increase in tropospheric O_3 volume mixing ratio compared to their *PiClim-2VOC* experiments. Furthermore, across all four models, the tropospheric O_3 volume mixing ratio of the *PiClim-NO$_x$* experiment surpasses that of the *PiClim-VOC* experiment, indicating the models' ability to accurately replicate the impact of rising anthropogenic emissions on O_3 production. Additionally, methane, a crucial natural source of volatile organic compounds and a key greenhouse gas, enhances tropospheric O_3 generation by CH_4 oxidation and influencing temperature, thereby elevating global O_3 volume mixing ratio. This phenomenon contributes to the heightened sensitivity of O_3 to methane volume mixing ratio in a clean atmosphere. Elevated volume mixing ratios of HCFCs (*PiClim-HC*) and nitrous oxide (*PiClim-N$_2$O*) lead to substantial stratospheric O_3 depletion, consequently affecting tropospheric O_3 volume mixing ratio through the pod coil process. Other influencing factors, such as aerosols and black carbon, induce warming through radiation effects, thereby simulating elevated O_3 volume mixing ratio.

Table 3. The averaged volume mixing ratio of global stratospheric ozone at all simulated vertical levels in the 29th and 30th year for each experiment of four models (ppbv).

Model \ *PiClim-*	*2xNOx*	*2xVOC*	*HC*	*CH4*	*NOx*	*VOC*	*NTCF*	*N2O*	*O3*	*aer*	*control*	*BC*
CESM2-WACCM	726.06	725.95	662.71	713.80	728.61	727.06	725.42	710.94				
GFDL-ESM4	628.63	626.68	571.32		632.03	628.92			632.70	628.44	629.98	629.78
GISS-E2-1-G	490.91	482.13	422.65	493.27	490.22	480.93	486.46	471.84	485.17	486.54	484.76	484.82
UKESM1-0-LL	707.27	707.93	613.89	697.32	716.14	704.78	723.99	694.44	714.27	697.04	702.88	701.81

Table 4. The averaged volume mixing ratio of global tropospheric ozone in the 29th and 30th year for each experiment of four models (ppbv).

Model \ PiClim-	*2xNOx*	*2xVOC*	*HC*	*CH4*	*NOx*	*VOC*	*NTCF*	*N2O*	*O3*	*aer*	*control*	*BC*
CESM2-WACCM	38.17	38.58	33.44	39.42	39.16	39.14	41.33	38.10				
GFDL-ESM4	31.33	31.62	24.42		32.64	32.25			34.09	31.01	30.79	30.95
GISS-E2-1-G	52.30	50.96	44.18	53.08	52.14	50.21	51.65	48.36	52.47	50.36	49.27	50.02
UKESM1-0-LL	47.53	46.14	31.04	45.55	46.02	45.97	47.29	45.04	46.65	43.69	46.70	45.11

Figure 3 shows the temporal evolution of tropospheric O_3 levels across various latitudes, as simulated by four distinct models in O_3 precursor experiments. In the *PiClim* experiments, none of the models predicted an enhancement in O_3 volume mixing ratio with simulation time at all latitudes, reflecting the consistent chemical lifetime of O_3 within the pristine atmospheric conditions. However, discrepancies in O_3 predictions among the models become more pronounced with increasing latitudes. While the CESM model generally exhibits higher tropospheric O_3 volume mixing ratios compared to the GFDL model, it paradoxically portrays the lowest O_3 levels in the equatorial region. The GISS model demonstrates a marked disparity in tropospheric O_3 volume mixing ratios between the Antarctic and Arctic regions, with the former registering notably higher levels. In contrast, the CESM and GFDL models exhibit similar patterns in this regard. A unique feature of the GISS model is a notable declining trend in Antarctic tropospheric O_3 levels during the initial 15 years of both the *PiClim-2VOC* and *PiClim-VOC* experiments. This trend is not observed in the CESM, GFDL, and UKESM models, highlightingthe sensitivity of the GISS model to precursors in simulating ozone is still higher than that of other models even in the pre-industrial clean atmosphere. The same conclusion was reached for NO_x experiments, but the ozone forcing was less than that in the VOC experiments. The UKESM model stands out with its pronounced simulation of elevated O_3 volume mixing ratios in the tropical belt. Furthermore, the *PiClim-2xVOC* experiment conducted within the UKESM model demonstrates a significant O_3 response to enhanced emissions of VOCs from natural sources in the equatorial region. This suggests a strong sensitivity of O_3 in the UKESM to increases in VOC emissions from natural sources.

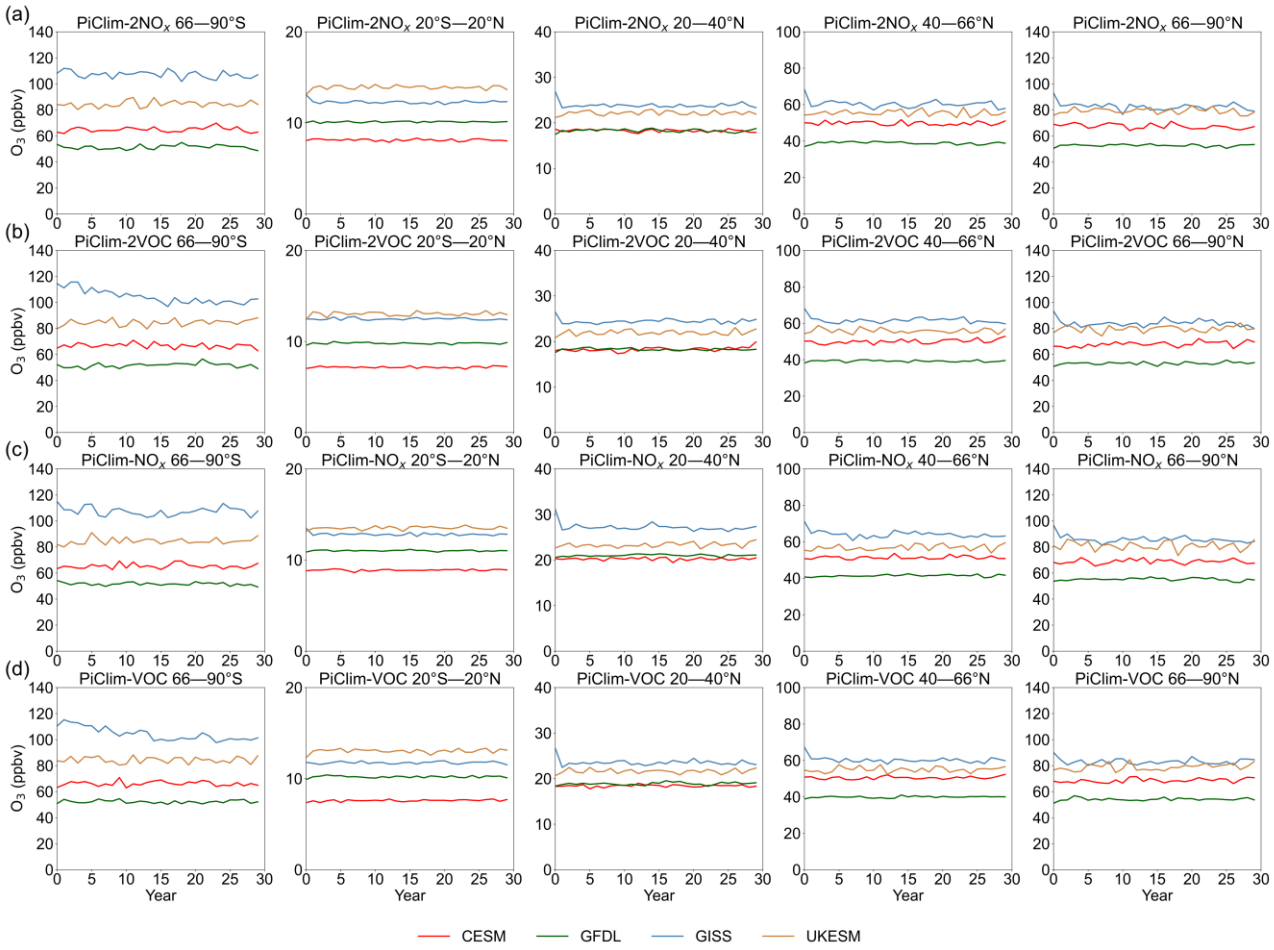

396

397 **Figure 3.** The temporal evolution characteristics of annual mean tropospheric column averaged O_3 volume mixing ratio at different latitudes for
398 each model are presented for the (a) *PiClim-2NO$_x$*, (b) *PiClim-2VOC*, (c) *PiClim-NO$_x$*, and (d) *PiClim-VOC* experiment, the 4 models are
399 represented by different line colors.

3.3 Analysis of O_3 generation in precursor experiments

In the shown subset of *PiClim* experiments, the O_3 production was defined as the cumulative tendency from HO_2, CH_3O_2, RO_2, and NO reactions, while O_3 loss encompassed the sum of O(1D) + H_2O, O_3 + HO_2, OH + O_3, and O_3 + alkene reactions. Figure 4 depicts the chemical production and consumption of tropospheric ozone in the five simulations performed by the four models. The GISS demonstrates the lowest O_3 chemical production among the models, whereas the other three models show generally consistent production levels. Notably, the GISS model exhibits a relatively low efficiency in O_3 chemical consumptions, primarily due to missing the loss of O_3 with isoprene and terpenes process. The low offset of ozone production and depletion in the pre-industrial atmosphere by the GISS model provides a new perspective based on previous studies indicating the high offset of ozone production and depletion in the present atmosphere by the GISS model. The four models all showed high ozone chemical production in the *PiClim-NO_x* experiment, indicating that the four all have perfect ability to simulate the photochemical generation mechanism of tropospheric ozone. However, the CESM and GFDL models do not show a significant increase in tropospheric O_3 chemical generation during the *PiClim-2NO_x* experiment. And although the GISS and UKESM models successfully simulated an increase in the O_3 chemical generation rate due to heightened lightning activity in this experiment, these increases in ozone production are also much smaller than the chemical production generated by the *PiClim-NO_x* experiment, which might show that the theoretical mechanism of ozone sensitivity to natural precursors in pre-industrial atmosphere differs from the present mechanism due to the differences in the characteristics of intermediate products such as OH. Furthermore, in either model, the ozone chemical production from the *PiClim-NO_x* experiment, while higher than in other experiments other than *PiClim-NTCF*, is much smaller than the ozone chemical production caused by this emission inventory in the atmosphere today (Fig. S5). Today's NO_x emission forcing has not led to a sustained increase in the ozone volume mixing ratio in the pre-industrial atmosphere over a long-time scale, which indicates important differences between the pre-industrial atmosphere and the present atmosphere in terms of the ozone generation environment and the ozone depletion environment.

Furthermore, the *PiClim-2VOC* experiment in the CESM and GFDL models lead to an increase in tropospheric O_3 volume mixing ratio, despite not reproducing higher

O_3 chemical production. The UKESM model successfully captures the enhancement of O_3 chemical formation due to increased emissions of VOCs from natural sources, underscoring its precise sensitivity to these emissions and validating its capability to simulate O_3 dynamics influenced by them. However, the global O_3 volume mixing ratio in the *PiClim-2xVOC* experiment of these models is lower than that of the *PiClim-VOC* experiment. These observations illustrate the variability among models in capturing the O_3 response to its precursor species, stemming from varied treatments of critical atmospheric processes, including photolysis, dry deposition, transport mechanisms, and mixing dynamics. Furthermore, these findings highlight the variability in global O_3 sensitivity compared to local O_3 sensitivity, underscoring the complexity of studying O_3 sensitivity on a global scale to mitigate its climate impacts.

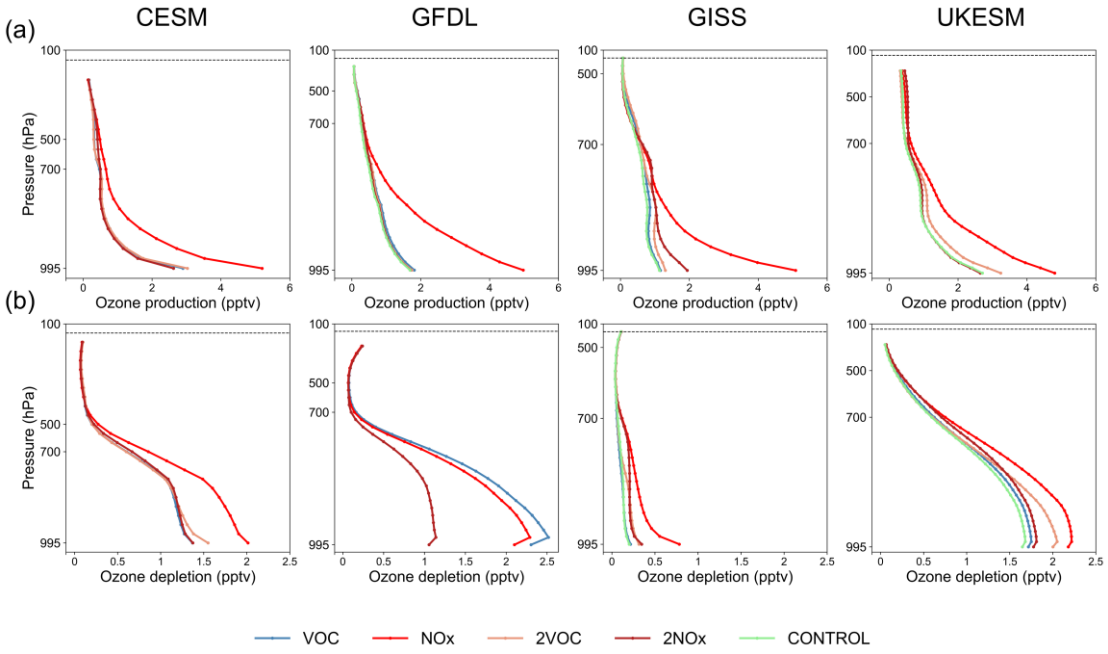

Figure 4. Vertical profiles of O_3 volume mixing ratio (a) chemical production and (b) chemical depletion rate for the 30th year across five experiments in the four models.

Figure 4b illustrates that, apart from the O_3 chemical formation mechanism, the CESM, GFDL, and UKESM models in the *PiClim-2NO$_x$* experiment do not accurately depict the O_3 chemical depletion process induced by NO_x. Despite successfully replicating the rise in NO and NO_2 levels (Fig. 5a, b) in the upper troposphere, these models fall short in capturing the NO_x-related O_3 depletion phenomenon. Moreover, the GISS model stands out with notably elevated NO_x volume mixing ratios attributed to heightened lightning activity compared to the other models. Additionally, it demonstrates a peak NO_x volume mixing ratio near 500 hPa across these four experiments conducted, a feature not observed in the other models.

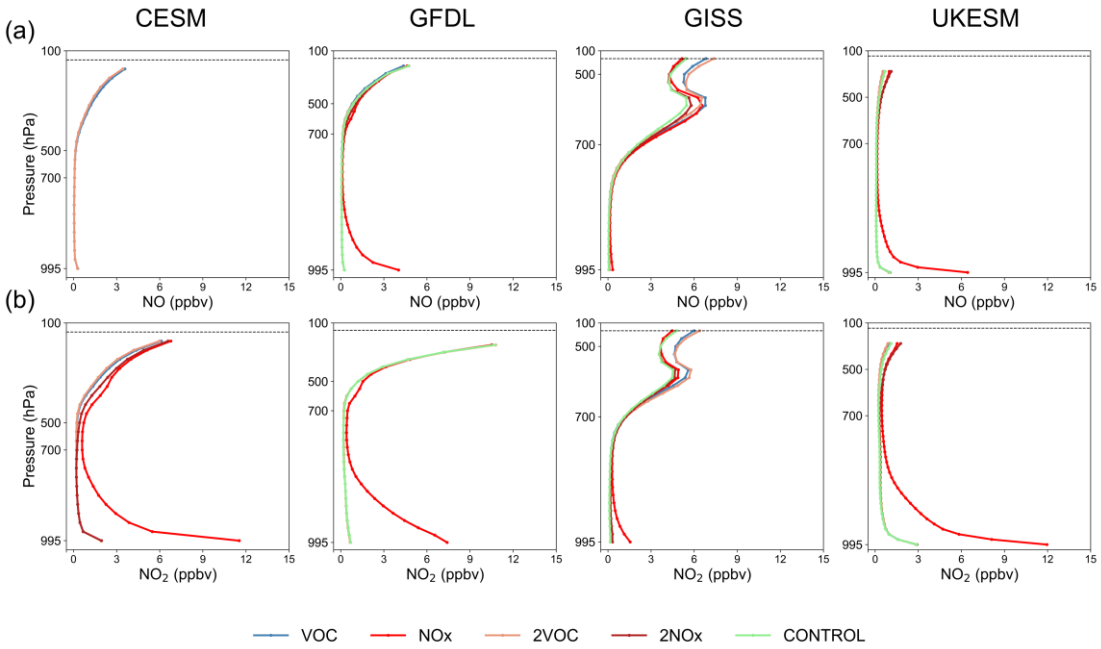

Figure 5. Vertical profiles of (a) NO and (b) NO_2 volume mixing ratios for the 30th year across five experiments in the four models.

Figure 6 illustrates a notable inverse correlation between the consumption of isoprene and the chemical production of O_3 in four models, when the rise in VOCs emissions is not factored in. This relationship is attributed to the significance of isoprene as a natural VOC source in unpolluted atmospheres and highlights the absence of O_3 generation simulation due to lightning activity in the CESM, GFDL, and UKESM models. In the *PiClim* experiments, the UKESM model did not provide mass fraction of secondary particulate organic matter dry aerosol particles in the air (mmrsoa), and so we only include its volume mixing ratio of isoprene in the air (isop) and the primary emissions and chemical production of dry aerosol organic matter (emioa) in Fig. 6. Additionally, the CESM model exhibits higher emissions and chemical formation of organic dry aerosol particles compared to the GFDL and GISS models. This difference potentially contributes to the observed variation in global O_3 volume mixing ratios, with the highest levels recorded in the CESM model and the lowest in the GISS model.

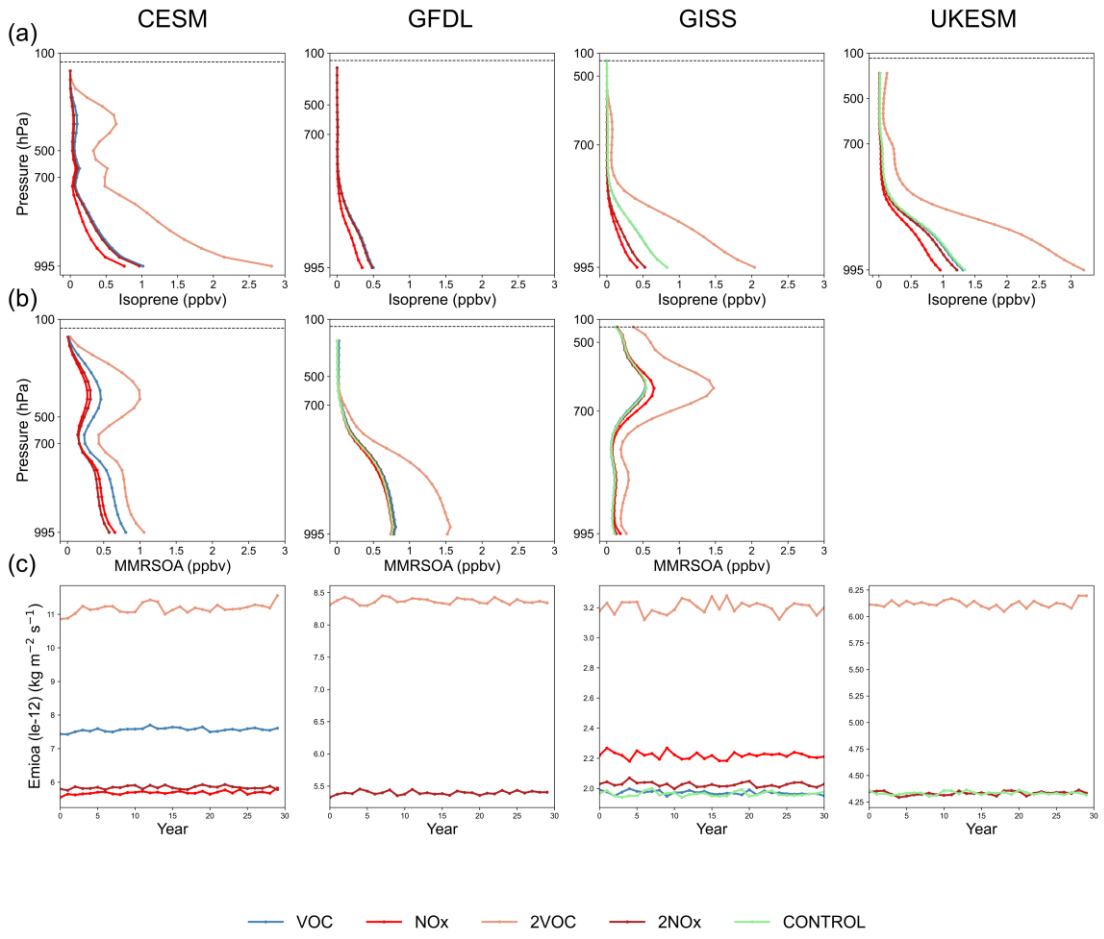

Figure 6. Vertical profiles of (a) isoprene volume mixing ratio and (b) secondary organic aerosol mass mixing ratio for the 30th year of all available experiments across the three models. (c) Temporal evolution characteristics of major emissions and the chemical production of organic dry aerosol particles from five experiments of the four models.

4. Conclusions

This study assessed the sensitivity of global-scale ozone (O_3) to precursor gases in a clean atmosphere and evaluated the simulation capabilities of four Earth system models using data from the *PiClim* experiments within the AerChemMIP framework. Our results highlight both strengths and limitations of these models in capturing O_3 response. The CESM and GFDL models excelled in reproducing seasonal O_3 cycles and the vertical distribution of O_3, but they showed limitations in simulating the tropospheric O_3 response to NO_x emissions from natural sources, such as lightning activity. Conversely, the GISS and UKESM models effectively simulated the positive correlation between tropospheric O_3 and temperature but were less sensitive to natural precursors compared to anthropogenic sources. Discrepancies, such as zonal

temperature biases in the GISS model and stratospheric temperature inconsistencies in the GFDL model, underscore areas for improvement.

Our findings suggest that existing assumptions regarding O_3 sensitivity to natural precursors may require refinement in clean atmospheric conditions. This research provides critical insights into the interplay between O_3 and its precursors, enhancing the accuracy of O_3 simulations in Earth system models. Given the significant role of O_3 in radiative forcing, atmospheric oxidation, and climate feedback mechanisms, our study reinforces the necessity of precise modeling to better predict and mitigate future climate scenarios. Additionally, the results underscore the importance of controlling anthropogenic precursor emissions as an essential strategy to manage tropospheric O_3 volume mixing ratios and address broader climate change challenges. Furthermore, among the models analyzed, only the GISS model demonstrates a significant increase in Antarctic ozone levels compared to the Arctic (Fig. 3); the other three models yield similar ozone concentrations at both polar regions. This discrepancy seems to result from a distinct characteristic of the GISS model's dynamical representation of the Antarctic polar vortex. Figure 1 also reveals that the ozone difference in the GISS model is predominantly confined to JJA and SON (Antarctic winter-spring).

It is important to acknowledge that the results generated by the models are accompanied by a degree of uncertainty.Variations in the methodologies employed by different models to address chemical reactions, including the production and depletion of ozone, contribute to the uncertainty surrounding the ozone budget. Furthermore, discrepancies in the data pertaining to anthropogenic and natural emissions, particularly concerning NO_x and BVOC emissions, substantially influence the outcomes of these models. Additionally, the uncertainty associated with the stratosphere-troposphere exchange process represents a critical factor in the ozone budget, with notable divergences in the treatment of this process across various models.

Acknowledgement

We acknowledge the World Climate Research Programme, which, through its Working Group on Coupled Modelling, coordinated and promoted CMIP6. We thank the climate modelling groups for producing and making available their model output,

the Earth System Grid Federation (ESGF) for archiving the data and providing access, and the multiple funding agencies who support CMIP6 and ESGF. We acknowledge the AerChemMIP groups of the four models used in the study (Vaishali Naik and Larry Horowitz for the GFDL simulations, Susanne E. Bauer and Kostas Tsigaridis for the GISS simulations, Fiona O'Connor and Jonny Williams for the UKESM simulations, as well as Louisa K. Emmons for the NCAR simulations). Particularly, we are grateful to Dr. Vaishali Naik for her comments and suggestions during the revision of this manuscript. We also thank the editor and anonymous reviewers for their time and comments, which helped improve the quality of this work greatly.

Data availability

All data from the Earth system models used in this paper are available on the Earth System Grid Federation website and can be downloaded from https://esgf-index1.ceda.ac.uk/search/cmip6-ceda/ (last access: 4 July 2024, ESGF-CEDA, 2024).

Author contributions

WW and CYG provided data analysis and contributed to the writing and discussion of this paper.

Competing interests

The authors declare that they have no conflict of interest.

References

Archibald, A. T., O'Connor, F. M., Abraham, N. L., Archer-Nicholls, S., Chipperfield, M. P., Dalvi, M., Folberth, G. A., Dennison, F., Dhomse, S. S., Griffiths, P. T., Hardacre, C., Hewitt, A. J., Hill, R. S., Johnson, C. E., Keeble, J., Kohler, M. O., Morgenstern, O., Mulcahy, J. P., Ordonez, C., Pope, R. J., Rumbold, S. T., Russo, M. R., Savage, N. H., Sellar, A., Stringer, M., Turnock, S. T., Wild, O., and Zeng, G.: Description and evaluation of the UKCA stratosphere-troposphere chemistry scheme (StratTrop vn 1.0) implemented in UKESM1, Geoscientific Model Development, 13, 1223-1266, 10.5194/gmd-13-1223-2020, 2020.

Austin, J., Horowitz, L. W., Schwarzkopf, M. D., Wilson, R. J., and Levy, H., II: Stratospheric ozone and temperature simulated from the preindustrial era to the present day, Journal of Climate, 26, 3528-3543, 10.1175/jcli-d-12-00162.1, 2013.

Bauer, S. E., Tsigaridis, K., Faluvegi, G., Kelley, M., Lo, K. K., Miller, R. L., Nazarenko, L., Schmidt, G. A., and Wu, J.: Historical (1850-2014) Aerosol evolution and role on climate forcing using the GISS ModelE2.1 contribution to CMIP6, Journal of Advances in Modeling Earth Systems, 12, 10.1029/2019ms001978, 2020.

Brown, F., Folberth, G. A., Sitch, S., Bauer, S., Bauters, M., Boeckx, P., Cheesman, A. W., Deushi, M., Dos Santos, I., Galy-Lacaux, C., Haywood, J., Keeble, J., Mercado, L. M., O'Connor, F. M., Oshima, N., Tsigaridis, K., and Verbeeck, H.: The ozone-climate penalty over South America and Africa by 2100, Atmospheric Chemistry and Physics, 22, 12331-12352, 10.5194/acp-22-12331-2022, 2022.

Carrillo-Torres, E. R., Hernandez-Paniagua, I. Y., and Mendoza, A.: Use of combined observational-and model-derived photochemical indicators to assess the O_3-NO_x-VOC system sensitivity in urban areas, Atmosphere, 8, 10.3390/atmos8020022, 2017.

Coffman, E., Rappold, A. G., Nethery, R. C., Anderton, J., Amend, M., Jackson, M. A., Roman, H., Fann, N., Baker, K. R., and Sacks, J. D.: Quantifying multipollutant health impacts using the environmental benefits mapping and analysis program-community edition (BenMAP-CE): A case study in Atlanta, Georgia, Environment Health Perspect, 132, 37003, 10.1289/EHP12969, 2024.

Collins, W. J., Lamarque, J.-F., Schulz, M., Boucher, O., Eyring, V., Hegglin, M. I., Maycock, A., Myhre, G., Prather, M., Shindell, D., and Smith, S. J.: AerChemMIP: quantifying the effects of chemistry and aerosols in CMIP6, Geoscientific Model Development, 10, 585-607, 10.5194/gmd-10-585-2017, 2017.

Dunne, J. P., Horowitz, L. W., Adcroft, A. J., Ginoux, P., Held, I. M., John, J. G., Krasting, J. P., Malyshev, S., Naik, V., Paulot, F., Shevliakova, E., Stock, C. A., Zadeh, N., Balaji, V., Blanton, C., Dunne, K. A., Dupuis, C., Durachta, J., Dussin, R., Gauthier, P. P. G., Griffies, S. M., Guo, H., Hallberg, R. W., Harrison, M., He, J., Hurlin, W., McHugh, C., Menzel, R., Milly, P. C. D., Nikonov, S., Paynter, D. J., Ploshay, J., Radhakrishnan, A., Rand, K., Reichl, B. G., Robinson, T., Schwarzkopf, D. M., Sentman, L. T., Underwood, S., Vahlenkamp, H., Winton, M., Wittenberg, A. T., Wyman, B., Zeng, Y., and Zhao, M.: The GFDL earth system model version 4.1 (GFDL-ESM 4.1): Overall coupled model description and simulation characteristics, Journal of Advances in Modeling Earth Systems, 12, 10.1029/2019ms002015, 2020.

Fowler, D., Pilegaard, K., Sutton, M. A., Ambus, P., Raivonen, M., Duyzer, J., Simpson, D., Fagerli, H., Fuzzi, S., Schjoerring, J. K., Granier, C., Neftel, A., Isaksen, I. S. A., Laj, P., Maione, M., Monks, P. S., Burkhardt, J., Daemmgen, U., Neirynck, J., Personne, E., Wichink-Kruit, R., Butterbach-Bahl, K., Flechard, C., Tuovinen, J. P., Coyle, M., Gerosa, G., Loubet, B., Altimir, N., Gruenhage, L., Ammann, C., Cieslik, S., Paoletti, E., Mikkelsen, T. N., Ro-Poulsen, H., Cellier, P., Cape, J. N., Horvath, L., Loreto, F., Niinemets, U., Palmer, P. I., Rinne, J., Misztal, P., Nemitz, E., Nilsson, D., Pryor, S., Gallagher, M. W., Vesala, T., Skiba, U., Brueggemann, N., Zechmeister-Boltenstern, S., Williams, J., O'Dowd, C., Facchini, M. C., de Leeuw, G., Flossman, A., Chaumerliac, N., and Erisman, J. W.: Atmospheric composition change: Ecosystems-atmosphere interactions, Atmospheric Environment, 43, 5193-5267, 10.1016/j.atmosenv.2009.07.068, 2009.

Gettelman, A., Hannay, C., Bacmeister, J. T., Neale, R. B., Pendergrass, A. G., Danabasoglu, G., Lamarque, J. F., Fasullo, J. T., Bailey, D. A., Lawrence, D. M., and Mills, M. J.: High climate sensitivity in the Community Earth System Model Version 2 (CESM2), Geophysical Research Letters, 46, 8329-8337, 10.1029/2019gl083978, 2019.

Griffiths, P. T., Murray, L. T., Zeng, G., Shin, Y. M., Abraham, N. L., Archibald, A. T., Deushi, M., Emmons, L. K., Galbally, I. E., Hassler, B., Horowitz, L. W., Keeble,

J., Liu, J., Moeini, O., Naik, V., O'Connor, F. M., Oshima, N., Tarasick, D., Tilmes, S., Turnock, S. T., Wild, O., Young, P. J., and Zanis, P.: Tropospheric ozone in CMIP6 simulations, Atmospheric Chemistry and Physics, 21, 4187-4218, 10.5194/acp-21-4187-2021, 2021.

Guenther, A., Hewitt, C. N., Erickson, D., Fall, R., Geron, C., Graedel, T., Harley, P., Klinger, L., Lerdau, M., Mckay, W. A., Pierce, T., Scholes, B., Steinbrecher, R., Tallamraju, R., Taylor, J., and Zimmerman, P.: A global model of natural volatile organic compound emissions, Journal of Geophysical Research-Atmospheres, 100, 8873-8892, https://doi.org/10.1029/94JD02950, 1995.

Guenther, A. B., Jiang, X., Heald, C. L., Sakulyanontvittaya, T., Duhl, T., Emmons, L. K., and Wang, X.: The Model of Emissions of Gases and Aerosols from Nature version 2.1 (MEGAN2.1): an extended and updated framework for modeling biogenic emissions, Geoscientific Model Development, 5, 1471-1492, 10.5194/gmd-5-1471-2012, 2012.

Hakim, Z. Q., Archer-Nicholls, S., Beig, G., Folberth, G. A., Sudo, K., Abraham, N. L., Ghude, S., Henze, D. K., and Archibald, A. T.: Evaluation of tropospheric ozone and ozone precursors in simulations from the HTAPII and CCMI model intercomparisons — a focus on the Indian subcontinent, Atmospheric Chemistry and Physics, 19, 6437-6458, 10.5194/acp-19-6437-2019, 2019.

Horowitz, L. W., Naik, V., Paulot, F., Ginoux, P. A., Dunne, J. P., Mao, J., Schnell, J., Chen, X., He, J., John, J. G., Lin, M., Lin, P., Malyshev, S., Paynter, D., Shevliakova, E., and Zhao, M.: The GFDL global atmospheric chemistry-climate model AM4.1: Model description and simulation characteristics, Journal of Advances in Modeling Earth Systems, 12, 10.1029/2019ms002032, 2020.

Hu, L., Wang, Z., Huang, M., Sun, H., and Wang, Q.: A remote sensing based method for assessing the impact of O_3 on the net primary productivity of terrestrial ecosystems in China, Frontiers in Environmental Science, 11, 10.3389/fenvs.2023.1112874, 2023.

Jin, X., Fiore, A. M., and Cohen, R. C.: Space-based observations of ozone precursors within California wildfire plumes and the impacts on ozone-NO_x-VOC chemistry, Environmental Science & Technology, 57, 14648-14660, 10.1021/acs.est.3c04411, 2023.

Karl, T., Lamprecht, C., Graus, M., Cede, A., Tiefengraber, M., de Arellano, J. V.-G., Gurarie, D., and Lenschow, D.: High urban NO_x triggers a substantial chemical downward flux of ozone, Science Advances, 9, 10.1126/sciadv.add2365, 2023.

Karset, I. H. H., Berntsen, T. K., Storelvmo, T., Alterskjaer, K., Grini, A., Olivie, D., Kirkevag, A., Seland, O., Iversen, T., and Schulz, M.: Strong impacts on aerosol indirect effects from historical oxidant changes, Atmospheric Chemistry and Physics, 18, 7669-7690, 10.5194/acp-18-7669-2018, 2018.

Kelley, M., Schmidt, G. A., Nazarenko, L. S., Bauer, S. E., Ruedy, R., Russell, G. L., Ackerman, A. S., Aleinov, I., Bauer, M., Bleck, R., Canuto, V., Cesana, G., Cheng, Y., Clune, T. L., Cook, B. I., Cruz, C. A., Del Genio, A. D., Elsaesser, G. S., Faluvegi, G., Kiang, N. Y., Kim, D., Lacis, A. A., Leboissetier, A., LeGrande, A. N., Lo, K. K., Marshall, J., Matthews, E. E., McDermid, S., Mezuman, K., Miller, R. L., Murray, L. T., Oinas, V., Orbe, C., Perez Garcia-Pando, C., Perlwitz, J. P., Puma, M. J., Rind,

D., Romanou, A., Shindell, D. T., Sun, S., Tausnev, N., Tsigaridis, K., Tselioudis, G., Weng, E., Wu, J., and Yao, M.-S.: GISS-E2.1: Configurations and climatology, Journal of Advances in Modeling Earth Systems, 12, 10.1029/2019ms002025, 2020.

Khomsi, K., Chelhaoui, Y., Alilou, S., Souri, R., Najmi, H., and Souhaili, Z.: Concurrent heat waves and extreme ozone (O_3) episodes: Combined atmospheric patterns and impact on human health, International Journal of Environmental Research and Public Health, 19, 10.3390/ijerph19052770, 2022.

Kumaş, K., Akyüz, A. J. I. J. o. E., and Geoinformatics: Estimation of greenhouse gas emission and global warming potential of livestock sector; Lake District, Türkiye, 2023.

Li, M., Huang, X., Yan, D., Lai, S., Zhang, Z., Zhu, L., Lu, Y., Jiang, X., Wang, N., Wang, T., Song, Y., and Ding, A.: Coping with the concurrent heatwaves and ozone extremes in China under a warming climate, Science Bulletin, 69, 2938-2947, https://doi.org/10.1016/j.scib.2024.05.034, 2024.

Lim, C. C., Hayes, R. B., Ahn, J., Shao, Y., Silverman, D. T., Jones, R. R., Garcia, C., Bell, M. L., and Thurston, G. D.: Long-term exposure to ozone and cause-specific mortality risk in the United States, American Journal of Respiratory and Critical Care Medicine, 200, 1022-1031, 10.1164/rccm.201806-1161OC, 2019.

Malley, C. S., Henze, D. K., Kuylenstierna, J. C. I., Vallack, H. W., Davila, Y., Anenberg, S. C., Turner, M. C., and Ashmore, M. R.: Updated global estimates of respiratory mortality in adults >=30 years of age attributable to long-term ozone exposure, Environment Health Perspect, 125, 087021, 10.1289/EHP1390, 2017.

Miller, R. L., Schmidt, G. A., Nazarenko, L. S., Tausnev, N., Bauer, S. E., DelGenio, A. D., Kelley, M., Lo, K. K., Ruedy, R., Shindell, D. T., Aleinov, I., Bauer, M., Bleck, R., Canuto, V., Chen, Y., Cheng, Y., Clune, T. L., Faluvegi, G., Hansen, J. E., Healy, R. J., Kiang, N. Y., Koch, D., Lacis, A. A., LeGrande, A. N., Lerner, J., Menon, S., Oinas, V., Garcia-Pando, C. P., Perlwitz, J. P., Puma, M. J., Rind, D., Romanou, A., Russell, G. L., Sato, M., Sun, S., Tsigaridis, K., Unger, N., Voulgarakis, A., Yao, M.-S., and Zhang, J.: CMIP5 historical simulations (1850-2012) with GISS ModelE2, Journal of Advances in Modeling Earth Systems, 6, 441-477, 10.1002/2013ms000266, 2014.

Möller, D. and Mauersberger, G.: Cloud chemistry effects on tropospheric photooxidants in polluted atmosphere — Model results, Journal of Atmospheric Chemistry, 14, 153-165, 10.1007/BF00115231, 1992.

Monks, P. S., Archibald, A. T., Colette, A., Cooper, O., Coyle, M., Derwent, R., Fowler, D., Granier, C., Law, K. S., Mills, G. E., Stevenson, D. S., Tarasova, O., Thouret, V., von Schneidemesser, E., Sommariva, R., Wild, O., and Williams, M. L.: Tropospheric ozone and its precursors from the urban to the global scale from air quality to short-lived climate forcer, Atmospheric Chemistry and Physics, 15, 8889-8973, 10.5194/acp-15-8889-2015, 2015.

Mulcahy, J. P., Jones, C., Sellar, A., Johnson, B., Boutle, I. A., Jones, A., Andrews, T., Rumbold, S. T., Mollard, J., Bellouin, N., Johnson, C. E., Williams, K. D., Grosvenor, D. P., and McCoy, D. T.: Improved aerosol processes and effective radiative forcing in HadGEM3 and UKESM1, Journal of Advances in Modeling Earth Systems, 10, 2786-2805, 10.1029/2018ms001464, 2018.

693 Murray, L. T., Logan, J. A., and Jacob, D. J.: Interannual variability in tropical
694 tropospheric ozone and OH: The role of lightning, Journal of Geophysical Research-
695 Atmospheres, 118, 11,468-411,480, https://doi.org/10.1002/jgrd.50857, 2013.

696 Naik, V., Horowitz, L. W., Fiore, A. M., Ginoux, P., Mao, J., Aghedo, A. M., and
697 Levy, H., II: Impact of preindustrial to present-day changes in short-lived pollutant
698 emissions on atmospheric composition and climate forcing, Journal of Geophysical
699 Research-Atmospheres, 118, 8086-8110, 10.1002/jgrd.50608, 2013a.

700 Naik, V., Voulgarakis, A., Fiore, A. M., Horowitz, L. W., Lamarque, J. F., Lin, M.,
701 Prather, M. J., Young, P. J., Bergmann, D., Cameron-Smith, P. J., Cionni, I., Collins,
702 W. J., Dalsøren, S. B., Doherty, R., Eyring, V., Faluvegi, G., Folberth, G. A., Josse,
703 B., Lee, Y. H., MacKenzie, I. A., Nagashima, T., van Noije, T. P. C., Plummer, D.
704 A., Righi, M., Rumbold, S. T., Skeie, R., Shindell, D. T., Stevenson, D. S., Strode,
705 S., Sudo, K., Szopa, S., and Zeng, G.: Preindustrial to present-day changes in
706 tropospheric hydroxyl radical and methane lifetime from the Atmospheric Chemistry
707 and Climate Model Intercomparison Project (ACCMIP), Atmospheric Chemistry and
708 Physics, 13, 5277-5298, 10.5194/acp-13-5277-2013, 2013b.

709 Nuvolone, D., Petri, D., and Voller, F.: The effects of ozone on human health,
710 Environmental Science and Pollution Research, 25, 8074-8088, 10.1007/s11356-017-
711 9239-3, 2018.

712 Pacifico, F., Harrison, S. P., Jones, C. D., Arneth, A., Sitch, S., Weedon, G. P.,
713 Barkley, M. P., Palmer, P. I., Serca, D., Potosnak, M., Fu, T. M., Goldstein, A., Bai,
714 J., and Schurgers, G.: Evaluation of a photosynthesis-based biogenic isoprene
715 emission scheme in JULES and simulation of isoprene emissions under present-day
716 climate conditions, Atmospheric Chemistry and Physics, 11, 4371-4389,
717 10.5194/acp-11-4371-2011, 2011.

718 Price, C. and Rind, D.: A simple lightning parameterization for calculating global
719 lightning distributions, Journal of Geophysical Research-Atmospheres, 97, 9919-
720 9933, https://doi.org/10.1029/92JD00719, 1992.

721 Price, C., Penner, J., and Prather, M.: NO_x from lightning: 1. Global distribution based
722 on lightning physics, Journal of Geophysical Research-Atmospheres, 102, 5929-5941,
723 https://doi.org/10.1029/96JD03504, 1997.

724 Price, C. G.: Lightning applications in weather and climate research, Surveys in
725 Geophysics, 34, 755-767, 10.1007/s10712-012-9218-7, 2013.

726 Rogelj, J., Schaeffer, M., Meinshausen, M., Shindell, D. T., Hare, W., Klimont, Z.,
727 Velders, G. J. M., Amann, M., and Schellnhuber, H. J.: Disentangling the effects of
728 CO_2 and short-lived climate forcer mitigation, Proceedings of the National Academy
729 of Sciences of the United States of America, 111, 16325-16330,
730 10.1073/pnas.1415631111, 2014.

731 Romanowsky, E., Handorf, D., Jaiser, R., Wohltmann, I., Dorn, W., Ukita, J., Cohen,
732 J., Dethloff, K., and Rex, M.: The role of stratospheric ozone for Arctic-midlatitude
733 linkages, Scientific Reports, 9, 7962, 10.1038/s41598-019-43823-1, 2019.

734 Schnell, J. L., Naik, V., Horowitz, L. W., Paulot, F., Mao, J., Ginoux, P., Zhao, M.,
735 and Ram, K.: Exploring the relationship between surface $PM_{2.5}$ and meteorology in

Northern India, Atmospheric Chemistry and Physics, 18, 10157-10175, 10.5194/acp-18-10157-2018, 2018.

Sellar, A. A., Jones, C. G., Mulcahy, J. P., Tang, Y., Yool, A., Wiltshire, A., O'Connor, F. M., Stringer, M., Hill, R., Palmieri, J., Woodward, S., de Mora, L., Kuhlbrodt, T., Rumbold, S. T., Kelley, D. I., Ellis, R., Johnson, C. E., Walton, J., Abraham, N. L., Andrews, M. B., Andrews, T., Archibald, A. T., Berthou, S., Burke, E., Blockley, E., Carslaw, K., Dalvi, M., Edwards, J., Folberth, G. A., Gedney, N., Griffiths, P. T., Harper, A. B., Hendry, M. A., Hewitt, A. J., Johnson, B., Jones, A., Jones, C. D., Keeble, J., Liddicoat, S., Morgenstern, O., Parker, R. J., Predoi, V., Robertson, E., Siahaan, A., Smith, R. S., Swaminathan, R., Woodhouse, M. T., Zeng, G., and Zerroukat, M.: UKESM1: Description and evaluation of the UK earth system model, Journal of Advances in Modeling Earth Systems, 11, 4513-4558, 10.1029/2019ms001739, 2019.

Shindell, D. T., Faluvegi, G., Unger, N., Aguilar, E., Schmidt, G. A., Koch, D. M., Bauer, S. E., and Miller, R. L.: Simulations of preindustrial, present-day, and 2100 conditions in the NASA GISS composition and climate model G-PUCCINI, Atmospheric Chemistry and Physics, 6, 4427-4459, 10.5194/acp-6-4427-2006, 2006.

Shindell, D. T., Pechony, O., Voulgarakis, A., Faluvegi, G., Nazarenko, L., Lamarque, J. F., Bowman, K., Milly, G., Kovari, B., Ruedy, R., and Schmidt, G. A.: Interactive ozone and methane chemistry in GISS-E2 historical and future climate simulations, Atmospheric Chemistry and Physics, 13, 2653-2689, 10.5194/acp-13-2653-2013, 2013.

Sillman, S. and He, D.: Some theoretical results concerning O_3-NO_x-VOC chemistry and NO_x-VOC indicators, Journal of Geophysical Research-Atmospheres, 107, ACH 26-21-ACH 26-15, https://doi.org/10.1029/2001JD001123, 2002.

Sporre, M. K., Blichner, S. M., Karset, I. H. H., Makkonen, R., and Berntsen, T. K.: BVOC-aerosol-climate feedbacks investigated using NorESM, Atmospheric Chemistry and Physics, 19, 4763-4782, 10.5194/acp-19-4763-2019, 2019.

Stevenson, D. S., Young, P. J., Naik, V., Lamarque, J. F., Shindell, D. T., Voulgarakis, A., Skeie, R. B., Dalsoren, S. B., Myhre, G., Berntsen, T. K., Folberth, G. A., Rumbold, S. T., Collins, W. J., MacKenzie, I. A., Doherty, R. M., Zeng, G., van Noije, T. P. C., Strunk, A., Bergmann, D., Cameron-Smith, P., Plummer, D. A., Strode, S. A., Horowitz, L., Lee, Y. H., Szopa, S., Sudo, K., Nagashima, T., Josse, B., Cionni, I., Righi, M., Eyring, V., Conley, A., Bowman, K. W., Wild, O., and Archibald, A.: Tropospheric ozone changes, radiative forcing and attribution to emissions in the Atmospheric Chemistry and Climate Model Intercomparison Project (ACCMIP), Atmospheric Chemistry and Physics, 13, 3063-3085, 10.5194/acp-13-3063-2013, 2013.

Stevenson, D. S., Dentener, F. J., Schultz, M. G., Ellingsen, K., van Noije, T. P. C., Wild, O., Zeng, G., Amann, M., Atherton, C. S., Bell, N., Bergmann, D. J., Bey, I., Butler, T., Cofala, J., Collins, W. J., Derwent, R. G., Doherty, R. M., Drevet, J., Eskes, H. J., Fiore, A. M., Gauss, M., Hauglustaine, D. A., Horowitz, L. W., Isaksen, I. S. A., Krol, M. C., Lamarque, J. F., Lawrence, M. G., Montanaro, V., Müller, J. F., Pitari, G., Prather, M. J., Pyle, J. A., Rast, S., Rodriguez, J. M., Sanderson, M. G., Savage, N. H., Shindell, D. T., Strahan, S. E., Sudo, K., and Szopa, S.: Multimodel ensemble

781 simulations of present-day and near-future tropospheric ozone, Journal of
782 Geophysical Research-Atmospheres, 111, 10.1029/2005jd006338, 2006.

783 Tilmes, S., Visioni, D., Jones, A., Haywood, J., Seferian, R., Nabat, P., Boucher, O.,
784 Bednarz, E. M., and Niemeier, U.: Stratospheric ozone response to sulfate aerosol
785 and solar dimming climate interventions based on the G6 Geoengineering Model
786 Intercomparison Project (GeoMIP) simulations, Atmospheric Chemistry and Physics,
787 22, 4557-4579, 10.5194/acp-22-4557-2022, 2022.

788 Unger, N.: On the role of plant volatiles in anthropogenic global climate change,
789 Geophysical Research Letters, 41, 8563-8569,
790 https://doi.org/10.1002/2014GL061616, 2014.

791 van Marle, M. J. E., Kloster, S., Magi, B. I., Marlon, J. R., Daniau, A. L., Field, R.
792 D., Arneth, A., Forrest, M., Hantson, S., Kehrwald, N. M., Knorr, W., Lasslop, G.,
793 Li, F., Mangeon, S., Yue, C., Kaiser, J. W., and van der Werf, G. R.: Historic global
794 biomass burning emissions for CMIP6 (BB4CMIP) based on merging satellite
795 observations with proxies and fire models (1750–2015), Geoscientific Model
796 Development, 10, 3329-3357, 10.5194/gmd-10-3329-2017, 2017.

797 Vermeuel, M. P., Novak, G. A., Alwe, H. D., Hughes, D. D., Kaleel, R. J., Dickens,
798 A., Kenski, D., Czarnetzki, A. C., Stone, E. A., Stanier, C. O., Pierce, R. B., Millet,
799 D. B., and Bertram, T. H. J. J. o. G. R. A.: Sensitivity of ozone production to NO_x
800 and VOC along the lake michigan coastline, Journal of Geophysical Research-
801 Atmospheres, 124, 10989 - 11006, 2019.

802 Walters, D., Baran, A. J., Boutle, I., Brooks, M., Earnshaw, P., Edwards, J., Furtado,
803 K., Hi, P., Lock, A., Manners, J., Morcrette, C., Mulcahy, J., Sanchez, C., Smith, C.,
804 Stratton, R., Tennant, W., Tomassini, L., Van Weverberg, K., Vosper, S., Willett, M.,
805 Browse, J., Bushell, A., Carslaw, K., Dalvi, M., Essery, R., Gedney, N., Hardiman,
806 S., Johnson, B., Johnson, C., Jones, A., Jones, C., Mann, G., Milton, S., Rumbold, H.,
807 Sellar, A., Ujiie, M., Whitall, M., Williams, K., and Zerroukat, M.: The met office
808 unified model global atmosphere 7.0/7.1 and JULES global land 7.0 configurations,
809 Geoscientific Model Development, 12, 1909-1963, 10.5194/gmd-12-1909-2019,
810 2019.

811 Williams, K. D., Copsey, D., Blockley, E. W., Bodas-Salcedo, A., Calvert, D., Comer,
812 R., Davis, P., Graham, T., Hewitt, H. T., Hill, R., Hyder, P., Ineson, S., Johns, T. C.,
813 Keen, A. B., Lee, R. W., Megann, A., Milton, S. F., Rae, J. G. L., Roberts, M. J.,
814 Scaife, A. A., Schiemann, R., Storkey, D., Thorpe, L., Watterson, I. G., Walters, D.
815 N., West, A., Wood, R. A., Woollings, T., and Xavier, P. K.: The met office global
816 coupled model 3.0 and 3.1 (GC3.0 and GC3.1) configurations, Journal of Advances
817 in Modeling Earth Systems, 10, 357-380, 10.1002/2017ms001115, 2018.

818 Young, P. J., Naik, V., Fiore, A. M., Gaudel, A., Guo, J., Lin, M. Y., Neu, J. L.,
819 Parrish, D. D., Rieder, H. E., Schnell, J. L., Tilmes, S., Wild, O., Zhang, L., Ziemke,
820 J., Brandt, J., Delcloo, A., Doherty, R. M., Geels, C., Hegglin, M. I., Hu, L., Im, U.,
821 Kumar, R., Luhar, A., Murray, L., Plummer, D., Rodriguez, J., Saiz-Lopez, A.,
822 Schultz, M. G., Woodhouse, M. T., and Zeng, G.: Tropospheric ozone assessment
823 report: assessment of global-scale model performance for global and regional ozone
824 distributions, variability, and trends, Elementa-Science of the Anthropocene, 6,
825 10.1525/elementa.265, 2018.

826 Zeng, G., Morgenstern, O., Williams, J. H. T., O'Connor, F. M., Griffiths, P. T.,
827 Keeble, J., Deushi, M., Horowitz, L. W., Naik, V., Emmons, L. K., Abraham, N. L.,
828 Archibald, A. T., Bauer, S. E., Hassler, B., Michou, M., Mills, M. J., Murray, L. T.,
829 Oshima, N., Sentman, L. T., Tilmes, S., Tsigaridis, K., and Young, P. J.: Attribution
830 of stratospheric and tropospheric ozone changes between 1850 and 2014 in CMIP6
831 models, Journal of Geophysical Research-Atmospheres, 127, 10.1029/2022jd036452,
832 2022.

833